Spin Frustration in $M^{II}[C(CN)_3]_2$ (M = V, Cr). A Magnetism and Neutron Diffraction Study

Jamie L. Manson,[†] Eric Ressouche,[‡] and Joel S. Miller*,[†]

Department of Chemistry, University of Utah, 315 South 1400 East RM 2124, Salt Lake City, Utah 84112-0850, and Département de Recherche Fondamentale sur la Matière Condensée, SPSMS-MDN, CEA/Grenoble, 17 rue des Martyrs, 38054 Grenoble Cedex 9, France

Received October 20, 1999

Three-dimensional coordination network solids of $M^{II}[C(CN)_3]_2$ (M = V, Cr) composition possess interpenetrating rutile-like network structures. Each $[C(CN)_3]^-$ bonds to three different metal ions in a triangular array, affording a geometrical topology akin to a Kagomé lattice leading to competing spin exchange interactions and spin frustration. The crystal and magnetic structure of $Cr^{II}[C(CN)_3]$ was determined by Rietveld refinement of the powder neutron diffraction data at 2 and 15 K and belongs to the orthorhombic space group *Pmna* [a = 7.313(1) Å, b = 5.453(1) Å, c = 10.640(1) Å, Z = 2, T = 15 K]. Each Cr^{II} has a tetragonally elongated octahedral structure with four Cr−N(1) distances of 2.077(2) Å and two significantly longer axial Cr−N(2) distances of 2.452(2) Å. Magnetic susceptibility measurements between 1.7 and 300 K reveal strong antiferromagnetic interactions for both V- and $Cr[C(CN)_3]_2$ with $\theta = -67$ and -46 K, respectively, from a fit to the Curie−Weiss law. Long-range magnetic ordering does not occur for M = V above 1.7 K, in contrast to M = Cr, which antiferromagnetically orders at low temperature. This is attributed to Jahn−Teller distorted Cr^{II} sites relieving frustration in one dimension, leading to 2-D Ising antiferromagnetism, as observed by both magnetic susceptibility and specific heat studies. Neutron diffraction experiments at 2 K for $Cr[C(CN)_3]_2$ yielded additional Bragg reflections as a result of antiferromagnetic ordering with the moments on the Cr^{II} atoms aligned parallel to c and 4.7(1) μ_B. Fitting of the magnetic order parameter to a power law yielded T_N = 6.12(4) K and β = 0.18(1) consistent with 2-D Ising behavior. A T_N of 6.13 K is also observed from the specific heat data.

Introduction

Multidimensional coordination solids composed of transition metals and polydentate organic bridging ligands constitute an important area of contemporary materials chemistry research. Numerous examples have been prepared and structurally characterized, as many of them possess interesting conducting[1a] and magnetic behaviors.[1b] Nitrile-containing organic ligands are particularly useful as they generally feature good Lewis basicity and provide efficient superexchange pathways between metal centers.[2,3] Recently, radical-based cyano acceptors such as tetracyanoethylene[1b,3] (TCNE) and 7,7,8,8-tetracyano-*p*-quinodimethane (TCNQ)[4] have received considerable interest since the molecule-based polymer, $V(TCNE)_x \cdot yCH_2Cl_2$, was discovered to magnetically order above room temperature.[5] One-dimensional chains or stacks found in [MnTPP][TCNE][3,6] [H_2TPP = *meso*-tetraphenylporphyrin] and $[Fe(C_5Me_5)_2]$-[TCNE],[1b,7] respectively, have been prepared and structurally characterized and are among the first molecule-based magnets. As part of our ongoing research on polynitrile-containing coordination compounds, we targeted metal complexes of the closed-shell D_{3h} tricyanomethanide, $[C(CN)_3]^-$, ligand due to its propensity to bind to three different metal sites. Reactions of paramagnetic M^{II} (M = V, Cr, Mn, Fe, Co, Ni, Cu) salts and $[C(CN)_3]^-$ in a 1:2 stoichiometry result in the formation of

[†] University of Utah.
[‡] CEA/Grenoble.

(1) (a) E.g.: *Handbook of conducting polymers*, 2nd ed.; Skotheim, T. A., Elsenbaumer, R. L., Reynolds, J. R., Eds.; M. Dekker: New York, 1998. *Handbook of organic conductive molecules and polymers*; Nalwa, H., Ed.; Wiley: New York, 1997. *Low-dimensional organic conductors*; Graja, A., World Scientific: Singapore, 1992. Ferraro, J. R.; Williams, J. M. *Introduction to synthetic electrical conductors*; Academic Press: Orlando, 1987. Hünig, S. *J. Mater. Chem.* **1995**, *5*, 1469. (b) Cassoux, P.; Miller, J. S. In *Chemistry of Advanced Materials: A New Discipline*; Interrante, L. V., Hampton-Smith, M. Eds.; VCH Publishers: New York, 1998; p 19. (c) E.g.: (a) Miller, J. S.; Epstein, A. J. *Angew. Chem., Int. Ed. Engl.* **1994**, *33*, 385. Miller, J. S.; Epstein, A. J. *Chem. Eng. News* **1995**, *73* (40), 30. Kinoshita, M. *Jpn. J. Appl. Phys.* **1994**, *33*, 5718. Gatteschi, D. *Adv. Mater.* **1994**, *6*, 635.

(2) (a) Ferlay, S.; Mallah, T.; Ouahes, R.; Veillet, P.; Verdaguer, M. *Nature* **1995**, *378*, 701. (b) Miyasaka, H.; Matsumoto, N.; Okawa, H.; Re, N.; Gallo, E.; Floriani, C. *Angew. Chem., Int. Ed. Engl.* **1995**, *34*, 1446. (c) Entley, W. R.; Girolami, G. S. *Science* **1995**, *268*, 397.

(3) Miller, J. S.; Epstein, A. J. *Chem. Commun. (Cambridge)* **1998**, 1319.

(4) Ouyang, X.; Campana, C.; Dunbar, K. R. *Inorg. Chem.* **1996**, *35*, 7188. Zhao, H.; Heintz, R. A.; Dunbar, K. R. *J. Am. Chem. Soc.* **1996**, *118*, 12844. Campana, C.; Dunbar, K. R.; Ouyang, X. *Chem. Commun. (Cambridge)* **1996**, 2427.

(5) Manriquez, J. M.; Yee, G. T.; McLean, R. S.; Epstein, A. J.; Miller, J. S. *Science* **1991**, *252*, 1415. Miller, J. S.; Yee, G. T.; Manriquez, J. M.; Epstein, A. J. In *Conjugated Polymers and Related Materials: The Interconnection of Chemical and Electronic Structure*; Proceedings of Nobel Symposium NS-81; Oxford University Press: Oxford, U.K., 1993; p 461; *Chem. Ind. (Milan)* **1992**, *74*, 845. Epstein, A. J.; Miller, J. S. In *Conjugated Polymers and Related Materials: The Interconnection of Chemical and Electronic Structure*; Proceedings of Nobel Symposium NS-81; Oxford University Press: Oxford, U.K., 1993; p 475; *Chem. Ind. (Milan)* **1993**, *75*, 185. Zhang, J.; Zhou, P.; Brinckerhoff, W. B.; Epstein, A. J.; Vazquez, C.; McLean, R. S.; Miller, J. S. *ACS Symp. Ser.* **1996**, *644*, 311.

(6) Miller, J. S.; Calabrese, J. C.; McLean, R. S.; Epstein, A. J. *Adv. Mater.* **1992**, *4*, 498.

(7) Miller, J. S.; Calabrese, J. C.; Rommelmann, H.; Chittipeddi, S. R.; Zhang, J. H.; Reiff, W. M.; Epstein, A. J. *J. Am. Chem. Soc.* **1987**, *109*, 769.

10.1021/ic991231d CCC: $19.00
Published on Web 02/23/2000

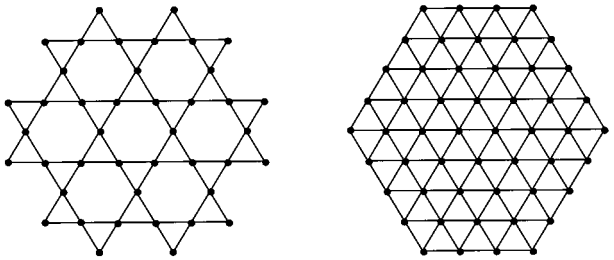

Figure 1. 2-D frustrating lattice types: Kagomé (left) and triangular (right).

interpenetrating rutile-type frameworks.[8] Here each metal site is three-connected to its nearest neighbors by the $[C(CN)_3]^-$ anion, affording triangular arrays analogous to what is observed for the prototypal inorganic network solid TiO_2 (rutile).[9]

Antiferromagnets based on 2-D triangular or Kagomé lattices, Figure 1, have received much attention from both theoretical and experimental points of view because of their fascinating characteristics.[10] This geometrical arrangement combined with competing interactions gives rise to spin-frustrated systems. Unfortunately, few compounds exist in which to study this phenomenon experimentally. Recently, a 2-D organic molecular solid composed of trigonally arranged $[m\text{-MPYNN}]^{\bullet+}[ClO_4]^-$ [MPYNN = *m*-*N*-methylpyridinium nitronyl nitroxide] was reported to exhibit spin frustration.[11] Thus, our main objectives were to deliberately design and prepare examples of coordination compounds that exhibit spin frustration. Herein, we report the synthesis, structure, magnetic properties, and neutron diffraction of $Cr[C(CN)_3]_2$, **1**, and $V[C(CN)_3]_2$, **2**.

Long-range magnetic ordering may be suppressed or significantly reduced as a result of competing antiferromagnetic interactions. Spin frustration is typically defined as a system's inability to simultaneously minimize energies associated with this competition.[12] Highly frustrated systems arise when the competing moments are of similar magnitude, leading to a large number of degenerate ground states. In other terms, an equilateral arrangement of equivalent spins is inherently frustrated because it is impossible to completely satisfy antiferromagnetic exchange interactions across more than two edges at the same time, Figure 1. When two spins are "satisfied", the third spin fluctuates and passes through a large number of excited states. Frustration may also be a consequence of disorder, which produces a random combination of both ferro- and antiferromagnetic interactions, ultimately leading to spin glass behavior. A square lattice may exhibit frustration if strong next-nearest-neighbor interactions exist, for example, in a site-disordered system. In the low-temperature regime, unusual magnetic properties are frequently observed and are often very difficult to predict. When absolute zero is approached, "spin liquids" may evolve where the spins are strongly interacting and fluctuating, in contrast to spin freezing which produces a static configuration.[13]

Experimentally, frustration is often identified by macroscopic properties. For an antiferromagnet, the critical temperature is defined by a singularity in the temperature dependence of the specific heat or the temperature derivative of the susceptibility, $\partial\chi/\partial T$. In a nonfrustrated system, the ordering temperature, T_N, and Weiss constant are of similar magnitude, *i.e.*, $T_N \sim |\theta|$, in contrast to a frustrated system where $T_N \ll |\theta|$. At high temperature, $1/\chi(T)$ should be strictly linear over a temperature range greater than θ. Deviation from linearity arises as a result of growing correlation length, a feature not associated with frustrated magnets. The degree of frustration can be quantified by eq 1. Frustration is present when $f > 1$, where $f > 10$ signifies

$$f = |\theta|/T_N \tag{1}$$

strong frustration.[14] As f increases, θ and T_N must respectively increase and decrease, leading to a suppressed critical temperature.

Experimental Section

Infrared Spectroscopy. Infrared spectra were recorded using a Bio-Rad FTS-40 FT IR spectrometer in the range 4000−600 cm^{-1} using Nujol mulls sandwiched between NaCl plates. The resolution of the instrument is ± 1 cm^{-1}.

X-ray Powder Diffraction. Room temperature X-ray powder diffraction patterns were collected on a Rigaku Miniflex X-ray diffractometer in the range $5° \le 2\theta \le 65°$ using a step size of 0.05° (40 s/step) and a wavelength of 1.5405 Å (Cu Kα). To perform the XRD studies on **1** and **2**, the samples were adhered to glass slides with high-vacuum grease and mounted vertically in an aluminum holder located in a home-built cell with a Mylar window and filled with an N_2 atmosphere.

Magnetic Measurements. Finely ground powdered samples of **1** and **2** were sealed in airtight Delrin holders and affixed to the end of a carbon fiber rod. Prior to sample insertion, the μ-metal shield was degaussed and the 5 T superconducting magnet reset to minimize residual dc fields. Dc magnetization and ac susceptibility measurements between 1.7 and 300 K and 2 and 40 K, respectively, were carried out using a Quantum Design MPMS-5XL AC/DC SQUID magnetometer equipped with continuous low temperature and temperature sweep modes, ultralow field, and reciprocating sample operation options. The samples were cooled in zero dc field to the lowest measured temperature (2 K) and data collected on warming. For the dc measurements, the samples were oscillated at 2 Hz using a 1 cm amplitude (RSO option) using an applied field of 1 kOe. Ac susceptibility was measured using a 1 Oe drive field oscillating at frequencies of 10, 100, and 1000 Hz. Temperature sweep rates of 0.5 and 0.1 K/min were utilized for the dc and ac measurements, respectively.

Neutron Powder Diffraction. The powder neutron diffraction experiments were carried out at the high flux reactor of the Institut Laue-Langevin (ILL, Grenoble), using the D1B and D20 position-sensitive diffractometers. The patterns were recorded between 2 and 15 K, using a top-loading liquid helium cryostat, using wavelengths of respectively 2.527 and 2.405 Å provided by focusing PG monochromators. The sample was enclosed in a cylindrical vanadium container 7 mm in diameter and 5 cm in height. Analyses of the neutron powder patterns were performed by Rietveld profile refinement using the software FULLPROF.[15] A Gaussian function was chosen to generate the line shape of the diffraction peaks. The scattering lengths were taken from Koester et al.,[16a] and the magnetic form factor of Cr was obtained from Brown.[16b]

(8) (a) Manson, J. L.; Campana, C.; Miller, J. S. *Chem. Commun. (Cambridge)* **1998**, 251. (b) Batten, S. R.; Hoskins, B. F.; Robson, R. *J. Chem. Soc., Chem. Commun*. **1991**, 445. (c) Enemark, J. H.; Holm, R. H. *Inorg. Chem*. **1964**, *3*, 1516.
(9) Wells, A. F. *Structural Inorganic Chemistry*; Oxford: New York, 1984; pp 14−15.
(10) Manousakis, E. *Rev. Mod. Phys.* **1991**, *63*, 1.
(11) (a) Awaga, K.; Okuno, T.; Yamaguchi, A.; Hasegawa, M.; Inabe, T.; Maruyama, Y.; Wada, N. *Phys. Rev. B* **1994**, *49*, 3975. (b) Awaga, K.; Okuno, T.; Yamaguchi, A.; Hasegawa, M.; Inabe, T.; Maruyama, Y.; Wada, N. *Synth. Met*. **1995**, *71*, 1807. (c) Wada, N. Kobayashi, T.; Yano, H.; Okuno, T.; Yamaguchi, A.; Awaga, K. *J. Phys. Soc. Jpn.* **1997**, *66*, 961.
(12) Clarke, S. J.; Fowkes, A. J.; Harrison, A.; Ibberson, R. M.; Rosseinsky, M. J. *Chem. Mater*. **1998**, *10*, 372.
(13) Schiffer, P.; Ramirez, A. P. *Comments Condens. Matter Phys*. **1996**, *18*, 21.
(14) Ramirez, A. P. *Annu. Rev. Mater. Sci.* **1994**, *24*, 453.
(15) Rodriguez-Carvajal, J. *Physica B* **1993**, *192*, 55.
(16) (a) Koester, L.; Rauch, H.; Seymann, E. *At. Data Nucl. Data Tables* **1991**, *49*, 65. (b) Brown, P. J. In *International Tables for Crystallography*; Wilson, A. J. C., Ed.; Kluwer: Dordrecht, 1992; pp 391−399.

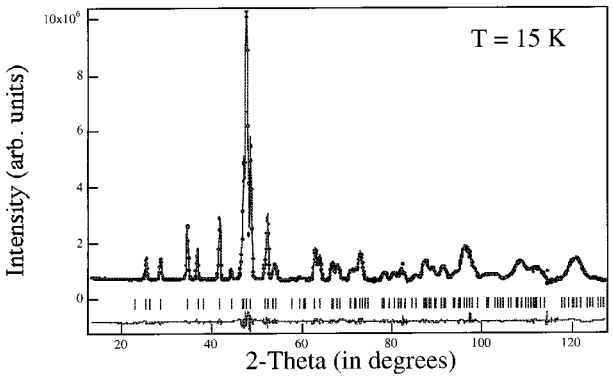

Figure 2. Observed and calculated powder neutron diffraction patterns at $T = 15$ K, as well as differences for **1**. The ticks indicate the positions of the nuclear reflections.

Specific Heat. The specific heat of a 2.1 mg pressed pellet of $Cr[C(CN)_3]_2$, **1**, was measured using a Quantum Design Physical Properties Measurement System (PPMS) equipped with a specific heat insert which uses a 2τ relaxation technique. Before the sample was mounted, the specific heat of the addenda plus adhesive (Apiezon "H" grease) was measured, and it this value was subtracted (during data acquisition) from the total specific heat during the following measurements with the sample mounted. The data were collected on cooling from 100 to 25 K every 3 K and from 24 to 2 K every 0.25 K. In another run, the data were measured from 14.8 to 4.8 K in increments of 0.1 K to enhance the resolution near T_N. The sample heating at each measurement point was 2% of the base temperature, with the relaxation measured for a duration of 2τ. Each point represents the average of two data points. The sample-to-addenda (heat capacity of the microcalorimeter chip, the bonded wires from the PPMS heat capacity stage, and adhesive) coupling was determined to be better than 94%. Thermal coupling between the sample and the sample holder was determined from the τ_2 model. It is given as a percentage with 100% corresponding to perfect thermal contact and 0% for no thermal contact.

Synthesis. All manipulations were carried out in a wet inert atmosphere Vacuum Atmospheres Drilab using degassed doubly distilled water.

$Cr[C(CN)_3]_2$, 1. A 15 mL aqueous solution of $K[C(CN)_3]$ (Alfa) (0.7881 g, 6.0 mmol) was added to a vigorously stirring aqueous solution of $Cr^{II}_2(O_2CMe)_4 \cdot 2H_2O$ (Aldrich) (0.5464 g, 1.5 mmol), giving immediate precipitation of a sky blue microcrystalline solid. To ensure complete reaction, the mixture was stirred for an additional 2 h. The material was collected via vacuum filtration, washed with copious amounts of fresh degassed H_2O, and dried in vacuo for 3 h (0.2996 g, 85%). ν_{CN} (Nujol): 2260 (s) and 2200 (vs) cm^{-1}.

$V[C(CN)_3]_2$, 2. An 8 mL aqueous solution of $K_2V^{II}(SO_4)_2 \cdot 6H_2O$[18] (0.4420 g, 1.0 mmol) was added to a vigorously stirring aqueous solution of $K[C(CN)_3]$ (0.2661 g, 2.0 mmol), giving a dark blue reaction mixture. After a few minutes, an olive green solid precipitated from solution and was collected via vacuum filtration, washed several times with fresh degassed water, and dried in vacuo for 5 h (0.1966 g, 82%). ν_{CN} (Nujol): 2245 (w, sh) and 2188 (s, br) cm^{-1}.

Results and Discussion

Crystal Structure. The crystal structure of **1** was elucidated by Rietveld refinement of the powder neutron diffraction data at 2 and 15 K. The diffraction pattern recorded in the paramagnetic state ($T = 15$ K), Figure 2, is consistent with the overall crystal structure reported for isostructural $Mn[C(CN)_3]_2$.[8a] All reflections at 15 K can be indexed to the orthorhombic space group *Pmna*, with $a = 7.313(1)$ Å, $b = 5.453(1)$ Å, and $c = 10.640(1)$ Å. The atomic positions were refined starting from the values observed in the manganese derivative. A summary of crystallographic data is presented in Table 1. As observed for $M[C(CN)_3]_2$ (M = Mn,[8a] Zn[8b]) each Cr^{2+} site is bonded to six N's of six different $[C(CN)_3]^-$ ligands, Figure 3, and each $[C(CN)_3]^-$ ligand is μ_3-bonded to three different Cr^{2+} ions, Figure 4. The structure is a 3-D rutile (TiO_2) lattice[9] where each Cr^{2+} and $[C(CN)_3]^-$ replaces Ti^{4+} and O^{2-}, respectively. Due to the formation of large pores, sufficient volume is available to allow interpenetration of a second equivalent network, Figure 4.

Unlike Mn^{II} and Zn^{II}, high-spin Cr^{2+} ion is expected to undergo Jahn−Teller distortion as observed. The tetragonally elongated octahedron has four equatorial Cr−N(1) distances of

Table 1. Crystallographic and Magnetic Structure Data of $Cr^{II}[C(CN)_3]$, **1**, Determined from a Rietveld Refinement of the Neutron Powder Diffraction

cell params (Å)		
T (K)	15 K	2 K
Z	2	2
a (Å)	7.3133(6)	7.3130(6)
b (Å)	5.4534(5)	5.4534(5)
c (Å)	10.6396(9)	10.6394(9)
Cr: 2b (0,0,$^1/_2$)		
magnetic moment (M_z)	0	4.7(1)
N(1): 8i (*x*,*y*,*z*)		
x	0.20597(43)	0.20600(42)
y	0.21430(46)	0.21424(45)
z	0.42659(23)	0.42661(23)
N(2): 4h (0,*y*,*z*)		
y	−0.23140(91)	−0.23100(90)
z	0.30458(32)	0.30464(32)
C(1): 8i (*x*,*y*,*z*)		
x	0.33811(66)	0.33823(65)
y	0.30346(64)	0.30334(63)
z	0.38915(37)	0.38920(37)
C(2): 4h (0,*y*,*z*)		
y	−0.39240(95)	−0.39197(93)
z	0.23547(54)	0.23563(53)
C(3): 4h ($^1/_2$,*y*,*z*+$^1/_2$)		
y	0.40714(107)	0.40742(105)
z+$^1/_2$	0.34729(51)	0.34726(50)
overall temp factor		
B	0.30(6)	0.29(6)
no. of reflns	106	106
no. of params	24	25
reliability factors		
R_p[a]	2.43	2.46
Rw_p[b]	3.53	3.54
Bragg *R*-factor (nuclear/magnetic)	2.22/0	2.04/30.4

[a] $R_p = \sum|I_{o_i} - I_{c_i}|/(\sum|I_{o_i}|)$. [b] $R_{wp} = [\sum w_i|I_{o_i} - I_{o_i}|^2/(\sum|I_{o_i}|^2)]^{1/2}$.

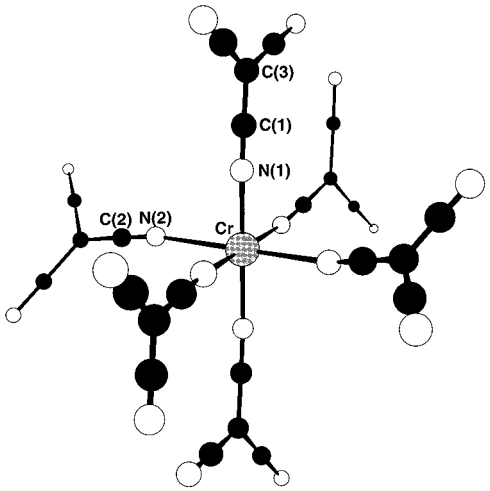

Figure 3. Local geometry of the Jahn−Teller distorted Cr^{II} octahedron observed in **1**. The Jahn−Teller axis is the Cr−N(2) one.

(17) Hwang, J. S.; Lin, K. J.; Tien, C. *Rev. Sci. Instrum.* **1997**, *68*, 94.
(18) $K_2V^{II}(SO_4)_2 \cdot 6H_2O$ was prepared according to the procedure of Cotton et al.: Cotton, F. A.; Falvello, L. R.; Llusar, R.; Libby, E.; Murillo, C. A.; Schwotzer, W. *Inorg. Chem.* **1986**, *25*, 3423.

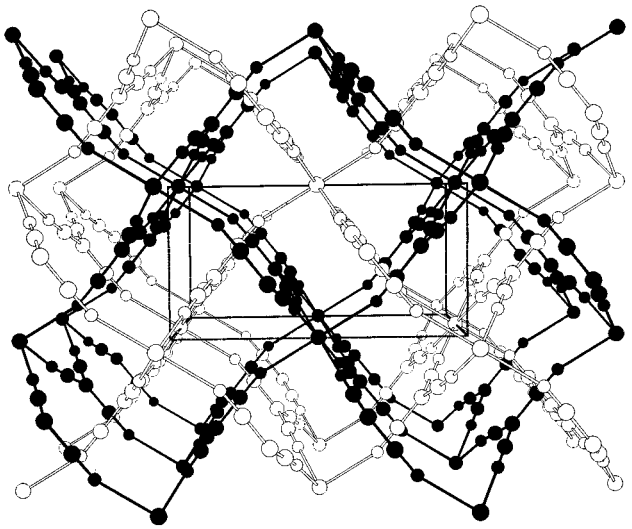

Figure 4. Space-filling view of $Cr[C(CN)_3]_2$, **1**. The two independent rutile-like networks are depicted as filled and open spheres, respectively.

2.077(2) Å and two significantly longer axial Cr−N(2) distances of 2.452(2) Å. This is a substantial distortion compared to isomorphous $Mn^{II}[C(CN)_3]_2$, which is only slightly elongated from octahedral symmetry with a difference in the Mn−N(1) and Mn−N(2) distances of 0.050 Å[8a] as opposed to a difference of 0.375 Å found for **1**. The C(1)−N(1) and C(2)−N(2) distances lie in the range typically observed in $[C(CN)_3]^-$ compounds.[8,19,20] Not only is the Cr^{2+} octahedron elongated but it is also squashed with *cis*-N−Cr−N′ bond angles ranging from 85.6(2)° to 94.4(2)°. Also, the $[C(CN)_3]^-$ ligands do not bind linearly to the metal with C(1)−N(1)−Cr and C(2)−N(2)−Cr bond angles of 170.3(2)° and 161.6(2)°, respectively, Figure 3. The basis for the 3-D structure is 1-D linear chains that propagate parallel to the *a*-axis, staggered *a*/2 relative to adjacent chains.

Due to the μ_3-N bonding of the $[C(CN)_3]^-$ ligand, metal ions are disposed onto a triangular array and provide a rare molecule-based example of a 3-D analogue of a 2-D triangular or Kagomé lattice,[21] Figure 1. In a single rutile-like network, Cr^{2+} sites lie at the vertices of an isosceles triangle with intranetwork Cr···Cr separations forming a side of 7.313 Å and two sides of 8.489 Å. The closest internetwork Cr···Cr separation is 5.453 Å and is nearly 2 Å shorter than the intranetwork distances.

In contrast, **2** is expected to be isotropic like $Mn[C(CN)_3]_2$ due to the nature of the d^3 V^{2+} ion with only unpaired electrons in the t_{2g} manifold. Other structures such as those of the pyrochlore, spinel, and other face-centered cubic varieties consist of corner- and/or edge-sharing tetrahedra have been shown to exhibit spin frustration.

X-ray powder diffraction of both **1** and **2** confirms their isostructural features, Figure 5. However, **1** gives strong, sharp Bragg peaks while **2** is poorly diffracting although the data is

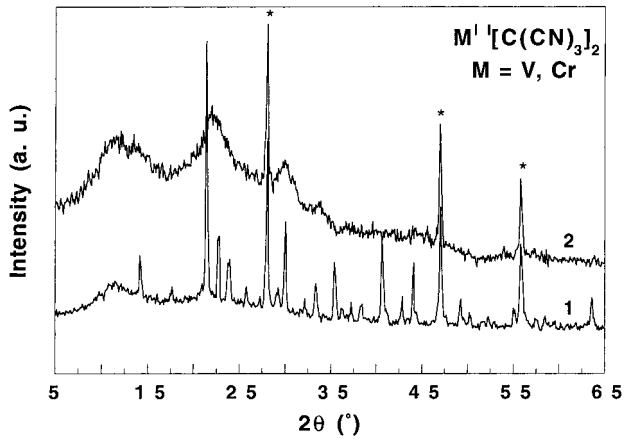

Figure 5. X-ray powder diffraction profiles of **1** and **2**. Asterisks mark the peaks associated with the internal Si standard.

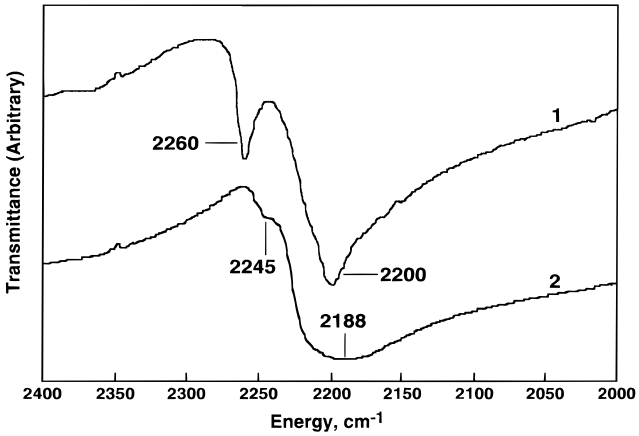

Figure 6. IR comparison of **1** and **2** taken as Nujol mulls.

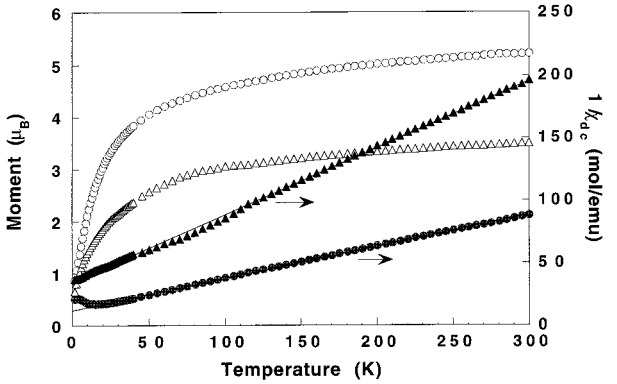

Figure 7. Temperature dependence of the effective moment, μ_{eff} (○, △), and reciprocal molar magnetic susceptibility, $1/\chi_{dc}$ (●, ▲), for **1** and **2**, respectively.

sufficient to identify its rutile-type structure. The degree of crystallinity is also reflected in the IR spectra, where **1** depicts two strong, sharp bands in the $\nu_{C\equiv N}$ region while **2** is strong but broadened, Figure 6. Furthermore, these broad features observed for **2** may be influenced by structural disorder and/or small particle size.

Magnetic Properties. The 2−300 K temperature dependence of the magnetic susceptibility, χ, of $S = 2$, **1**, and $S = {}^3/_2$, **2**, was fit by the Curie−Weiss expression, $\chi \propto (T - \theta)^{-1}$ with Landé *g*-values of 2.35 and 2.00 and θ values of −46 and −67 K, respectively, indicative of to significant antiferromagnetic coupling between metal sites, Figure 7. Below ∼80 K deviations from Curie−Weiss behavior due to the onset of single-ion

(19) Chow, Y. M.; Britton, D. *Acta Crystallogr.* **1975**, *B31*, 1934. Schiavo, S.; Bruno, G.; Zanello, P.; Laschi, F.; Piraino, P. *Inorg. Chem.* **1997**, *36*, 1004. Potocnák, I.; Dunaj-Jurco, M.; Miklos, D.; Jäger, L. *Acta Crystallogr.* **1996**, *C52*, 1653. Dixon, D. A.; Calabrese, J. C.; Miller, J. S. *J. Am. Chem. Soc.* **1986**, *108*, 2582.

(20) Wang, J.-C.; Shih, L. J.; Chen, Y.-J.; Wang, Y.; Fronczek, F. R.; Watkins, S. F. *Acta Crystallogr.* **1993**, *B49*, 680. Summerville, D. A.; Cohen, I. A.; Hatano, K.; Scheidt, W. R. *Inorg. Chem.* **1978**, *17*, 2906. Hvastijová, M.; Kozisek, J.; Kohout, J.; Jäger, L.; Fuess, H. *Transition Met. Chem.* **1995**, *20*, 276. Konnert, J.; Britton, D. *Inorg. Chem.* **1966**, *7*, 1193. Batten, S. R.; Hoskins, B. F.; Robson, R. *Angew. Chem., Int. Ed. Engl.* **1997**, *36*, 636.

(21) Syozi, I. *Prog. Theor. Phys.* **1951**, 6, 306.

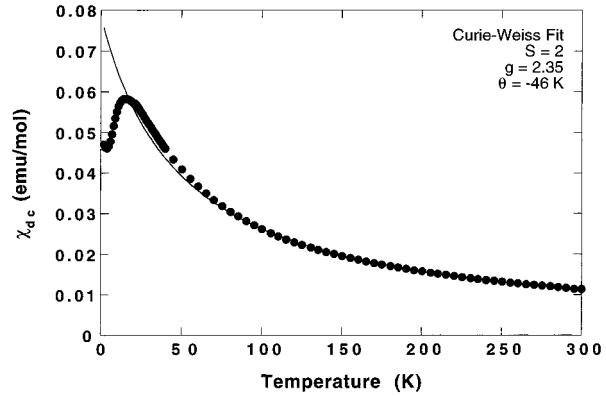

Figure 8. Temperature dependence of $\chi(T)$ showing the antiferromagnetic ordering of **1**. The solid line is the fit to the Curie−Weiss expression with $g = 2.30$ and $\theta = -46$ K.

anisotropy and short-range ordering is observed for **1**.[22] The 2.35 g-value for **1** is in good agreement with those reported for $[H_3N(CH_2Ph)]_2CrCl_4$[23a−c] and $Cr[N(CN)_2]_2$.[23d] At 300 K the effective moment for **1** is 5.38 μ_B, higher than expected for uncoupled $S = 2$ Cr^{2+} ions, but typical for this ion with Landé *g*-values that occasionally exceed 2.00,[24] while it is 3.50 μ_B and reduced from the 3.87 μ_B spin-only value for **2** due to stronger antiferromagnetic coupling. The moment of **1** decreases gradually to ∼50 K before falling off rapidly down to 2 K reaching a minimum value of 0.95 μ_B, Figure 7. For **2**, a minimum value of 0.67 μ_B is reached at the lowest attainable temperature of 1.7 K. Using the mean field theory and the Ising formalism to estimate the exchange coupling via the $[C(CN)_3]^-$ ligand, values for J/k_B of −1.9 and −2.7 K were obtained assuming the number of nearest neighbors (*z*) of 6 and 10 for **1** and **2**, respectively. A reduced *z* of 6 utilized for **1** does not consider the nearest magnetic neighbors located along the Jahn−Teller axis.

A transition to long-range magnetic order is suggested from the $\chi(T)$ and $d\chi T(T)/dT$ for **1**, Figure 8. $\chi(T)$ increases upon cooling from a value of 0.012 emu/mol until a maximum value of 0.058 emu/mol is reached at 15 K. Upon further cooling, $\chi(T)$ decreases rapidly down to 4 K reaching a value of 0.046 emu/mol before increasing slightly again to a value of 0.047 emu/mol at 2 K. Furthermore, the rounded maximum in $\chi(T)$ is reminiscent of a 2-D Ising lattice.[25] In-phase ac susceptibility, $\chi'(T)$, measurements being taken at frequencies of 10, 100, and 1000 Hz using a 1 Oe amplitude, is identical to that shown in Figure 8 and shows no frequency dependence as expected for an ordered antiferromagnet.[26] No out-of-phase, $\chi''(T)$, components were observed indicating a noncanted ground state.

High-spin Cr^{II} possesses a ^5E_g ground state and, as such, temperature-independent paramagnetism and spin−orbit coupling are small and may be neglected.[24] As discussed earlier, since the metal ions lie at the vertices of a triangular lattice, spin frustration may arise if antiferromagnetic coupling dominates. Due to effects of distortion, the triangular array is isosceles and not equilateral; nonetheless, spin frustration remains plausible, with fewer ground state degeneracies. The superexchange interaction is mediated through the −Cr−N≡C−Cr−C≡N−Cr− pathway. As the two Cr−N bonds in the *bc* plane are longer than the four other Cr−N bonds, the antiferromagnetic interaction along the *a* direction is expected to be stronger than those along the other two edges of the triangle. Hence an antiferromagnetic arrangement is satisfied in the *a* direction while frustration remains in the other two directions, leading to the observed long-range magnetic order at 6 K for **1**. According to eq 1, $f = 5.1$ for **1**, suggesting moderate frustration.

Table 2. Comparison of Magnetic Properties for Selected Spin-Frustrated Materials

compound	magnetic lattice	θ (K)	T_N (K)	f, $\lvert\theta\rvert/T_N$	ref
$MnIn_2Te_4$	zinc blende	−100	4	25	29
K_2IrCl_6	fcc	−32.1	3.1	10.5	30
$[Co(NH_3)_6][FeCl_6]$	fcc	−4.6	0.5	9.2	31
VCl_2	triangular	−437	36	12	27
$NaTiO_2$	triangular	−1000	<2	>500	12, 32
$SrCr_8Ga_4O_{19}$	kagome	−515	3.5	150	33
[*m*-MPYNN][ClO_4]	kagome	−3.1	<0.030	>103	11
$ZnCr_2O_4$	β-spinel	−390	16	24	34
$Mn[C(CN)_3]_2$	triangular	−5.1	1.18	4.3	8a
$Cr[C(CN)_3]_2$	triangular	−46	9	5.1	this work
$V[C(CN)_3]_2$	triangular	−67	<1.7	>40	this work

Evidence for long-range magnetic order is not present for **2** due to the lack of deviation from Curie−Weiss behavior above 1.7 K, suggesting $T_N \ll 1.7$ K. Due to the anticipated low ordering temperature and the extreme air sensitivity of **2**, additional experiments such as specific heat and neutron diffraction which could be used to determine T_N cannot be performed at present. $\chi_{ac}(T)$ gives behavior analogous to that of $\chi_{dc}(T)$ and shows no evidence of frequency dependence, as expected for a magnetically coupled system above T_N. In contrast to **1**, $f > 40$ indicative of very strong frustration is observed. This *f*-value can be compared to values observed in other materials, Table 2. The VX_2 (X = Cl, Br, I) family of V^{II} triangular-lattice antiferromagnets, which possess the 2-D CdI_2 type structure, have large negative θ-values of −437 (Cl), −335 (Br), and −143 K (I) and antiferromagnetically order below 36.0 (Cl), 29.5 (Br), and 16.3 (I) K, respectively.[27] From this, *f*-values of 12, 11, and 9 for VCl_2, VBr_2, and VI_2, respectively, can be computed. These values represent moderate frustration in comparison to the significantly more frustrated **2** but are only slightly larger than that obtained for **1**. Examples of spin-frustrated systems are given in Table 2 along with their respective *f*, θ, and T_N values.

Isothermal magnetization measurements taken at 2 K for **1** and **2** have a nearly linear dependence as a function of increasing dc magnetic field (Figure 9). Due to strong antiferromagnetic interactions, saturation is not achieved and leads to values significantly reduced from the predicted values of 26 700 and 16 755 emuOe/mol for uncoupled spins of $S = 2$ and $^3/_2$, respectively. In the antiferromagnetically ordered state, small net magnetization values such as those observed for **1** and **2** of 2150 and 1260 emu Oe/mol, respectively, are expected due to random orientation of antiferromagnetic domains.

Magnetic Structure of $Cr[C(CN)_3]_2$, 1. Neutron scattering experiments carried out between 2 and 15 K in zero applied field were used to elucidate the magnetic structure of **1**, Figures

(22) Carlin, R. L. *Magnetochemistry*; Springer-Verlag: New York, 1981; pp 117−123.
(23) (a) Bellitto, C.; Day, P.; Wood, T. E. *J. Chem. Soc., Dalton Trans.* **1986**, 847. (b) Day, P. *Acc. Chem. Res.* **1979**, *14*, 236. (c) Bellito, C.; Day, P. *J. Mater. Chem.* **1992**, *2*, 265. (d) Manson, J. L.; Kmety, C. R.; Epstein, A. J.; Miller, J. S. *Inorg. Chem.* **1999**, *38*, 2552.
(24) Figgis, B. N. *Introduction to Ligand Fields*; Krieger: Malabar, 1986.
(25) (a) Fisher, M. E. *J. Math. Phys.* **1963**, *4*, 124. (b) Wada, N.; Kashima, Y.; Haseda, T.; Morosin, B. *J. Phys. Soc. Jpn.* **1981**, *50*, 3876.
(26) Mydosh, J. A. *Spin Glasses: An Experimental Introduction*; Taylor and Francis: London, 1993; Chapter 3.
(27) (a) Niel, M.; Cros, C.; Le Flem, G.; Pouchard, M.; Hagenmuller, P. *Physica* **1977**, *86−88B*, 702. (b) Hirakawa, K.; Kadowaki, H.; Ubukoshi, K. *J. Phys. Soc. Jpn.* **1983**, *52*, 1814.

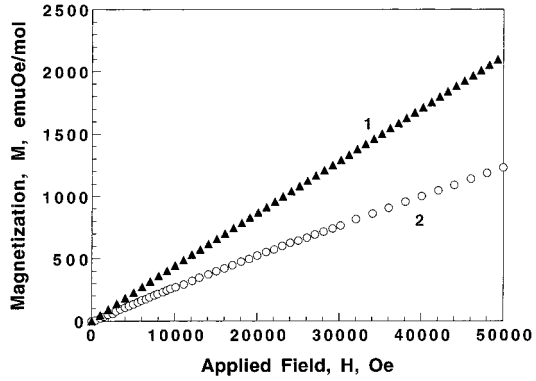

Figure 9. Isothermal magnetization of **1** and **2** recorded at 2 K.

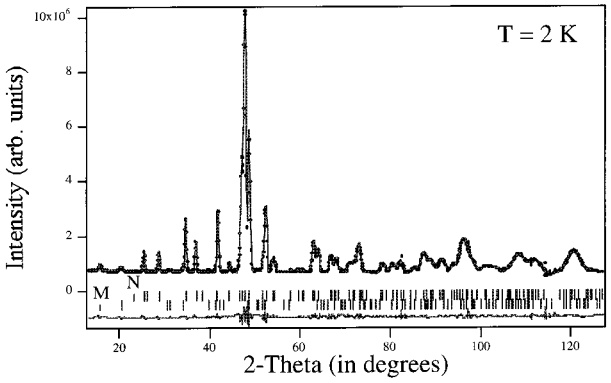

Figure 10. Observed and calculated powder neutron diffraction patterns at $T = 2$ K, as well as differences for **1**. The ticks indicate the positions of the reflections, for both the nuclear (N) and the magnetic (M) contributions.

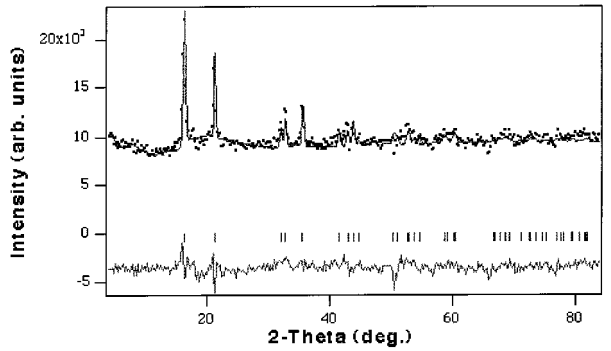

Figure 11. Difference plot between the 2 and 15 K neutron data for **1**, emphasizing the additional Bragg reflections below T_N due to magnetic scattering.

10 and 11. Antiferromagnetic ordering in the material manifests itself in the appearance of additional Bragg reflections at half-integer positions, giving a propagation vector $\kappa = [^1/_2\ ^1/_2\ 0]$. The magnetic structure ($2a \times 2b \times c$) is commensurate with the crystallographic structure. A full least-squares refinement including both nuclear and magnetic phases was carried out. The magnetic structure that leads to the best fit of the neutron data consists of moments on the Cr atoms aligned parallel to the *c* axis, Figure 12.

Several patterns were then recorded with increasing temperature up to 10 K and each analyzed by the Rietveld method. The temperature variation of the magnetic moment is provided in Figure 13. At 2 K the magnetic moment, M_z, is 4.7(1) μ_B, which is larger than the expected value of 4 μ_B ($\equiv 2S\mu_B$) due to the large *g*-value. The data was fit to a power law of the type $M \sim (T_N - T)^\beta$ yielding a Neel temperature, T_N, of 6.12(4) K and a critical exponent, β, of 0.18(1). The β-value obtained is

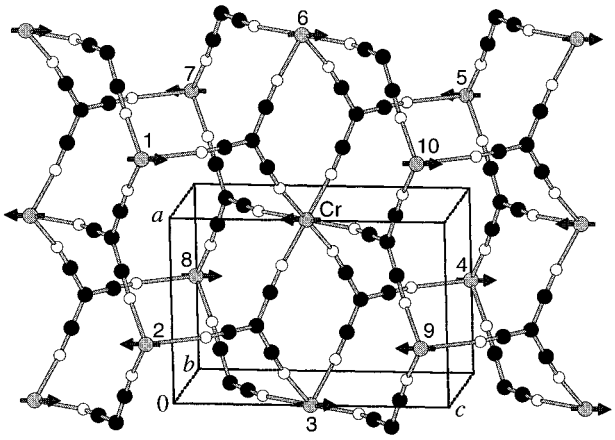

Figure 12. Illustration of the magnetic structure of a single lattice of **1** at 2 K. The arrows delineate the spin orientation of the ordered magnetic moment. The unit cell is outlined and only one interpenetrating network has been shown for clarity.

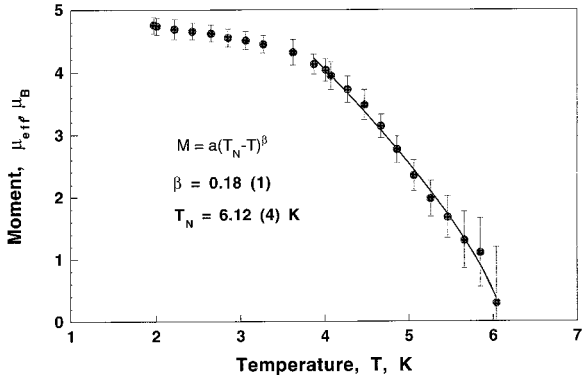

Figure 13. Variation of the Cr magnetic moment in **1** as a function of temperature. The solid line represents the best fit of the data to a power law giving $T_N = 6.12(4)$ K and $\beta = 0.18(1)$.

consistent with that of the 2-D Ising model (0.125).[25,28] The slightly larger β-value is likely a consequence of some residual 3-D interactions that perhaps should not be neglected. In contrast, **2** was not studied with neutrons as vanadium has a very small scattering length, rendering it nearly invisible to a neutron beam as far as nuclear scattering is concerned.[13]

Specific Heat of $Cr[C(CN)_3]_2$, 1. The temperature dependence of the specific heat, $C_p(T)$, of **1** was measured between 2 and 20 K, Figure 14. A broad maximum centered at ~10 K suggests strong 2-D correlations between the Cr sites and agrees with the results of the $\chi_{dc}(T)$ studies.[25] Upon close inspection of the region between 5 and 8 K, a subtle change in slope occurs near 6 K. To determine where the 3-D magnetic phase transition lies, a very good estimate could be made from the first derivative of the specific heat, $\partial C_p(T)/\partial T$, Figure 14 (inset). A change in slope, i.e., an inflection point, is readily observed at 6.13 K that signifies T_N.

(28) de Jongh, L. J.; Miedema, A. R. *Experiments on Simple Magnetic Model Systems*; Taylor and Francis: London, 1974.
(29) Döll, G.; Anghel, A.; Baumann, J. R.; Bucher, E.; Ramirez, A. P. Range, K. J. *Phys. Status Solidi* **1991**, *A126*, 237.
(30) Lines, M. E.; Jones, E. D. *Phys. Rev. B* **1966**, *141*, 525.
(31) Moron, M. C.; Palacio, F.; Navarro, R.; Pons, J.; Casabo, J.; Carlin, R. L. *Inorg. Chem.* **1990**, *29*, 842.
(32) Hirakawa, K.; Kadowaki, H.; Ubukoshi, K. *J. Phys. Soc. Jpn.* **1985**, *54*, 3526.
(33) Ramirez, A. P.; Espinosa, G. P.; Cooper, A. S. *Phys. Rev. Lett.* **1990**, *64*, 2070.
(34) Baltzer, P. K.; Wojtowicz, P. J.; Robbins, M.; Lopatin, E. *Phys. Rev.* **1966**, *151*, 367.

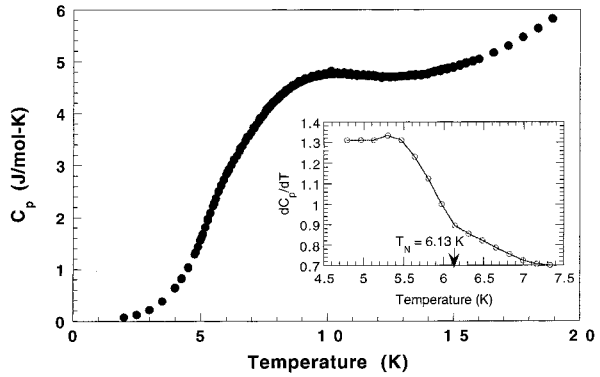

Figure 14. Specific heat of **1** taken between 2 and 20 K. Inset: Temperature dependence of the first derivative of the specific heat, $\partial C_p(T)/\partial T$, of **1**.

Conclusion

Incorporation of the triangular μ_3-$[C(CN)_3]^-$ ligand into polymeric arrays has led to a new class of spin-frustrated molecule-based magnets of the type $M^{II}[C(CN)_3]_2$ (M = V, Cr). The crystal structure of $Cr^{II}[C(CN)_3]_2$ was determined from neutron powder diffraction at low temperature and was found to adopt an interpenetrating rutile-like topology. Comparison of X-ray powder data of M = V and Cr suggests that they are isostructural, although Cr^{II} is Jahn−Teller distorted. From detailed magnetic measurements, $Cr[C(CN)_3]_2$ orders as an antiferromagnet below 6.12(4) K as confirmed by specific heat and neutron diffraction, while $V[C(CN)_3]_2$ does not order above 1.7 K. It is proposed that the Jahn−Teller active Cr^{II} sites relieve frustration in one dimension, consequently leading to 2-D Ising magnetic behavior as observed. This contrasts with isotropic V^{II} that displays very strong spin frustration in a manner frequently associated with transition metal oxides.

Acknowledgment. The authors gratefully acknowledge the American Chemical Society Petroleum Research Fund (Grant 30722-AC5) and the U.S. Department of Energy (Grant DE-FG03-93ER45504) for support of this work. E.R. would also like to thank P. Convert (Institut Laue-Langevin, ILL, Grenoble) for his help with neutron scattering experiments. J.L.M. and J.S.M. also acknowledge Prof. K. Awaga and Prof. N. Wada (Tokyo University) and D. Matien and D. Polancic (Quantum Design) for their assistance with the specific heat measurements.

IC991231D